Ambio

Electronic Supplementary Material

This supplementary material has not been peer reviewed.

Title: **Thawing permafrost and methane emission in Siberia: synthesis of observations, reanalysis, and predictive modelling**

Oleg Anisimov, Sergei Zimov

Evaluating the regional climatic changes in Russia using observational data.

Modern climatic changes in Russia are not uniform across space and through the seasons. Warming is more pronounced in the Russian Arctic and subarctic, including the permafrost regions, where the mean annual temperature is rising by 0.5–0.9°C per decade. The rate of warming differs by season and is the highest in the spring and in the summer (up to 1.0–1.2°C per decade in the North of Siberia) and moderate in the fall (0.4–0.6°C per decade with the least pronounced regional differences). Winter temperature changes have a complex regional pattern and range from a rise by 0.4–0.8°C per decade in Central and Northern Siberia, Yakutia and the Russian Far East, to a decline of 0.2–0.6°C per decade in southern Siberia and Chukotka. Annual sums of precipitation in the past four decades rose in most Russian regions at the average rate of 0.8 mm/month per decade with large interannual and regional variations.

We used data from the full set of Roshydromet weather stations to construct the large-scale pattern of modern climatic changes in different Russian regions. To minimize the stochastic component, which is present in the individual station records, we combined the records into groups and developed a climatic regionalization based on the coherence of the temperature variations. We tested several classifications consisting of different numbers of regions using data for different periods. The regional delineations were all based on the analysis of bio-climatic and topographic conditions. The optimal classification for the modern period is shown in Figure S1 and consists of 17 regions, 14 of which are in the Russian Federation, and the other are in the neighboring states. Five regions, (1, 7, 10, 11, and 12 in Fig. S1) span the permafrost zone. Figure S2 illustrates temperature variations in each region.

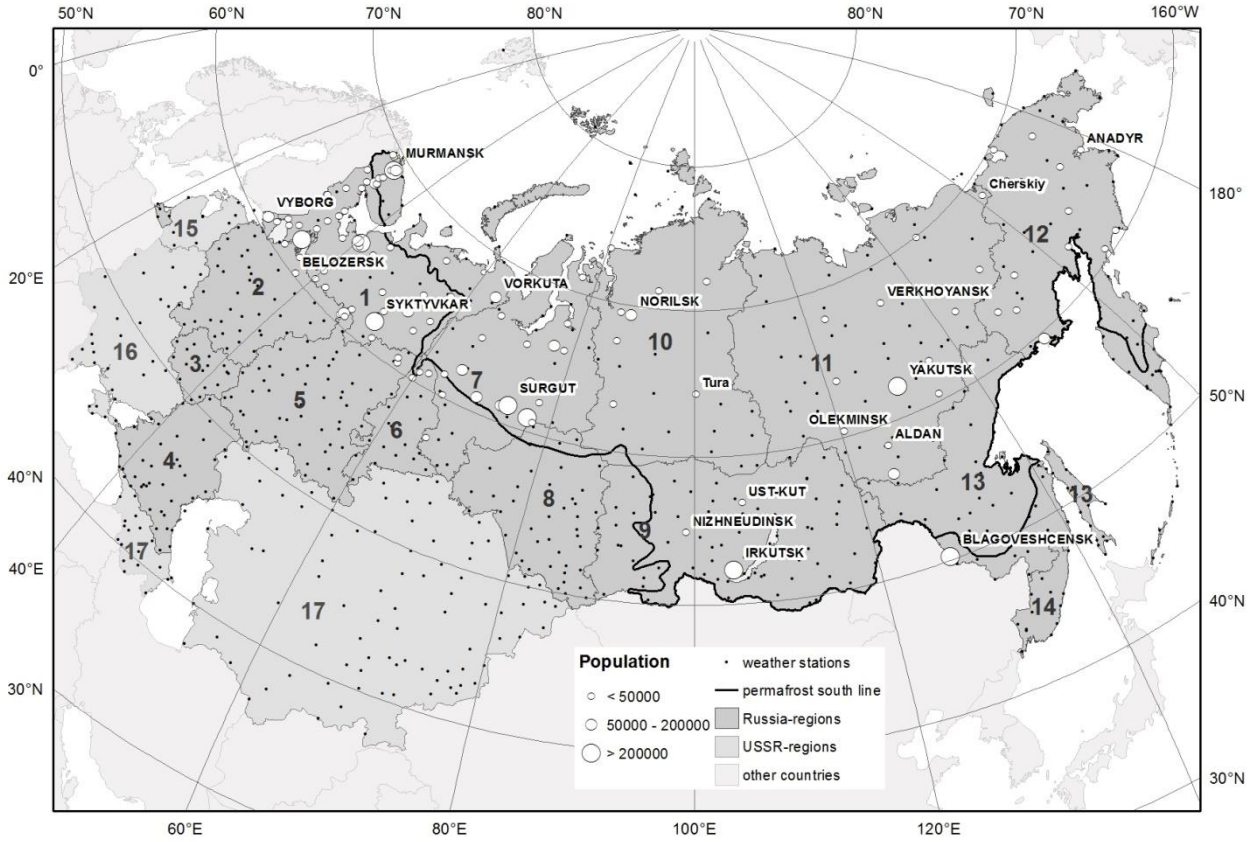

Fig. S1. Regions with coherent contemporaneous temperature changes.

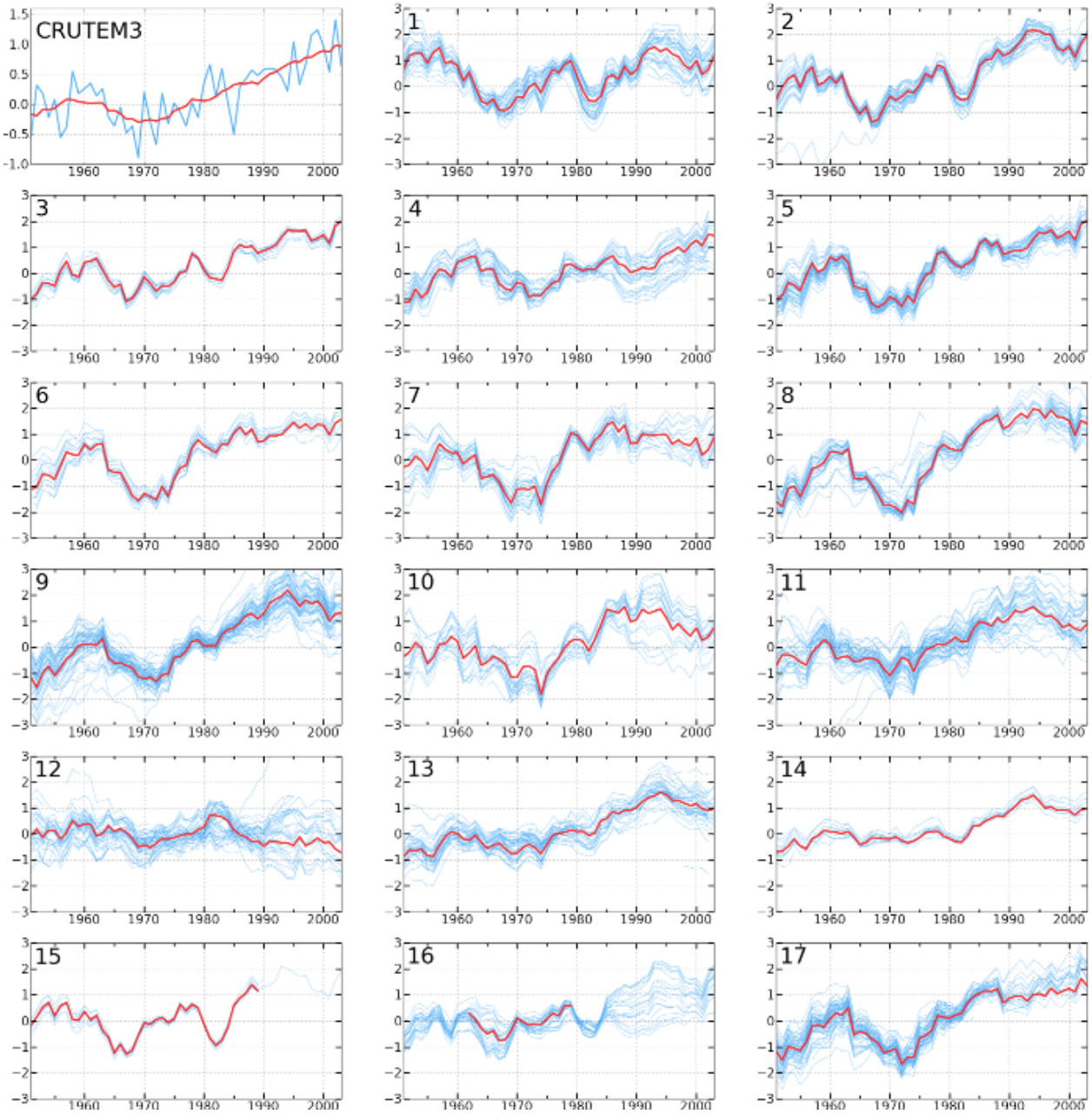

Fig. S2. Temperature variations at individual stations (thin blue lines) and regional-mean MAAT (red lines) smoothed with an 11-year running filter.

Optimal ensemble climate projection for Russian permafrost regions

Following our earlier study (Anisimov and Kokorev 2017), we constructed the optimal climate projection for the Russian permafrost region. The projection is based on results from the so-called CMIP5 generation of the Earth System Models (ESMs), which were used in the Fifth IPCC report. Climate Models Intercomparison Project (CMIP5) was detailed in (Taylor et al. 2011). CMIP5 computations include historical (for the period 1850 – 2005) and predictive (for

the period 2006 – 2100) runs. Results from different ESMs differ in details, and regional uncertainties in climate projections remain high (Flato et al. 2013).

Global climate models have a typical horizontal resolution of about 2° by latitude and longitude, which corresponds to a spatial unit with a size of 200-250 km. Complicating the problem, the results of any individual model for any single grid node are not robust, and the entire pattern contains many unreliable small-scale details, often interpreted as if it is affected by stochastic "noise" (Raisanen and Ylhaisi 2011). This imposes limitations for projecting climatic changes at specific locations, such as individual cities. Similar to observations at individual stations, "noise" may be reduced by averaging several neighboring grids (spatial smoothing), or by applying the same procedure to several models. The ensemble approach is used to minimize the uncertainty of the climate projections. While early studies postulated decreasing uncertainty with the increase in the number of models in the ensemble, more recent papers suggest eliminating outliers, i.e. GCMs that demonstrate poor performance in comparison with observations. Model discrimination and construction of optimal ensemble projections for regional studies could be based on the consistency with observations of the specific climatic parameters.

We used results from 36 CMIP5 climate models and evaluated each model's accuracy by comparing calculated trends in the climatic characteristics with observations in the 14 Russian regions. Tests have been performed using the 1976-2005 data for the seasonal and annual temperatures and sums of precipitation. Original data have been harmonized by subtracting the "baseline" values averaged over the 1961-1990 period individually for each model. This procedure eliminates systematic biases, which individual models are prone to. Results were averaged over the grid nodes that fall over each of the regions in Fig. S1, and compared with the regional observations. Ultimately, models were ranked according to their capability.

Model	Pfrost	1	7	9	10	11	12	13
ACCESS1.3	–1.5	–2.1	0.4	–3.4	–1.7	0.1	0.8	–1.8
ACCESS1–0	0.4	2.6	2.4	–1.7	0.1	0.0	2.5	–1.7
bcc–csm1–1	4.5	7.3	8.0	–2.1	3.9	1.5	–0.6	–0.7
bcc–csm1–1–m	–0.5	–2.4	–0.5	–2.9	0.2	2.8	5.0	2.7
BNU–ESM	0.4	–4.0	0.1	1.0	1.1	2.3	4.4	2.1
CanCM4	–0.2	2.8	2.3	–5.2	–1.2	–0.8	–0.2	–2.1
CanESM2	2.1	0.7	2.3	–1.3	1.1	1.0	3.4	1.0
CESM1–CAM5	–4.4	–5.1	–3.6	–2.8	–3.7	–2.3	–3.9	–3.9
CESM1–FASTCHEM	1.1	0.0	4.4	–2.9	3.8	1.9	–1.2	–1.6
CMCC–CESM	–2.7	–1.0	1.2	–4.7	–0.5	–2.8	–3.9	–5.8
CMCC–CM	1.4	2.3	4.1	4.0	3.3	1.0	–3.3	0.5
CMCC–CMS	–3.6	–5.6	–2.9	–1.2	–3.1	–2.3	–2.0	–1.8
CNRM–CM5	4.4	5.0	7.7	1.4	6.7	4.1	6.7	2.0
CSIRO–Mk3–6–0	0.2	–0.6	2.6	–1.4	1.6	–0.7	–0.8	0.2
EC–EARTH	1.6	–1.7	3.3	–0.9	3.2	0.7	0.6	2.1
FIO–ESM	–0.6	–3.6	2.8	–1.8	2.5	–0.1	–0.2	–2.4
GFDL–CM3	–3.2	–6.5	–1.2	–3.2	–2.9	–3.2	4.0	–1.7
GFDL–ESM2G	1.7	1.6	4.8	–1.4	3.3	3.6	7.4	1.5
GFDL–ESM2M	–1.0	–5.8	–0.6	–0.7	0.6	–0.3	–1.8	–0.8
GISS–E2–H	0.3	3.1	2.5	–4.2	0.1	–0.2	–1.3	0.0
GISS–E2–R	0.3	–0.7	2.2	–1.7	2.5	1.7	0.8	–0.7
HadCM3	1.3	3.0	2.3	–3.0	–0.2	4.1	2.6	0.9
HadGEM2–AO	2.0	1.3	5.3	1.4	5.8	3.4	1.1	0.6
HadGEM2–CC	1.5	–0.3	3.6	–3.0	1.1	1.0	2.3	0.7
HadGEM2–ES	3.0	1.8	2.8	0.4	2.9	3.9	3.9	2.3
inmcm4	–3.3	–5.6	–1.1	–5.3	–2.6	–3.9	–4.0	–4.6
IPSL–CM5A–LR	–1.0	–1.6	1.0	–0.1	–0.6	0.0	0.1	0.9
MIROC4h	–2.7	–3.5	–1.0	–1.8	–1.1	–0.5	–0.2	–2.8
MIROC–ESM	–2.4	–3.3	–0.4	–1.4	–0.6	–0.9	0.2	–0.6
MIROC–ESM–CHEM	0.4	0.5	2.8	–4.2	0.2	–1.9	–1.0	–2.6
MPI–ESM–LR	–3.8	–8.0	–2.7	–4.1	–3.4	–0.9	0.0	–0.5
MPI–ESM–MR	–0.3	–0.3	1.8	–2.1	0.2	0.9	2.5	–2.5
MPI–ESM–P	–1.1	–2.0	2.7	0.4	2.6	0.1	–1.3	–2.3
MRI–CGCM3	–4.6	–5.7	–3.6	–5.9	–3.6	–3.0	–1.4	–4.2
NorESM1–M	0.8	2.4	3.0	0.3	0.7	–0.3	3.8	0.0
NorESM1–ME	–2.9	0.7	1.5	–5.3	–3.8	–6.8	–3.9	–5.4

Table S1. Differences between the modeled MAAT trends and observations in the 1976-2005 period for selected regions in the Russian North, °C/100 years. Based on data from CMIP5 historical runs.

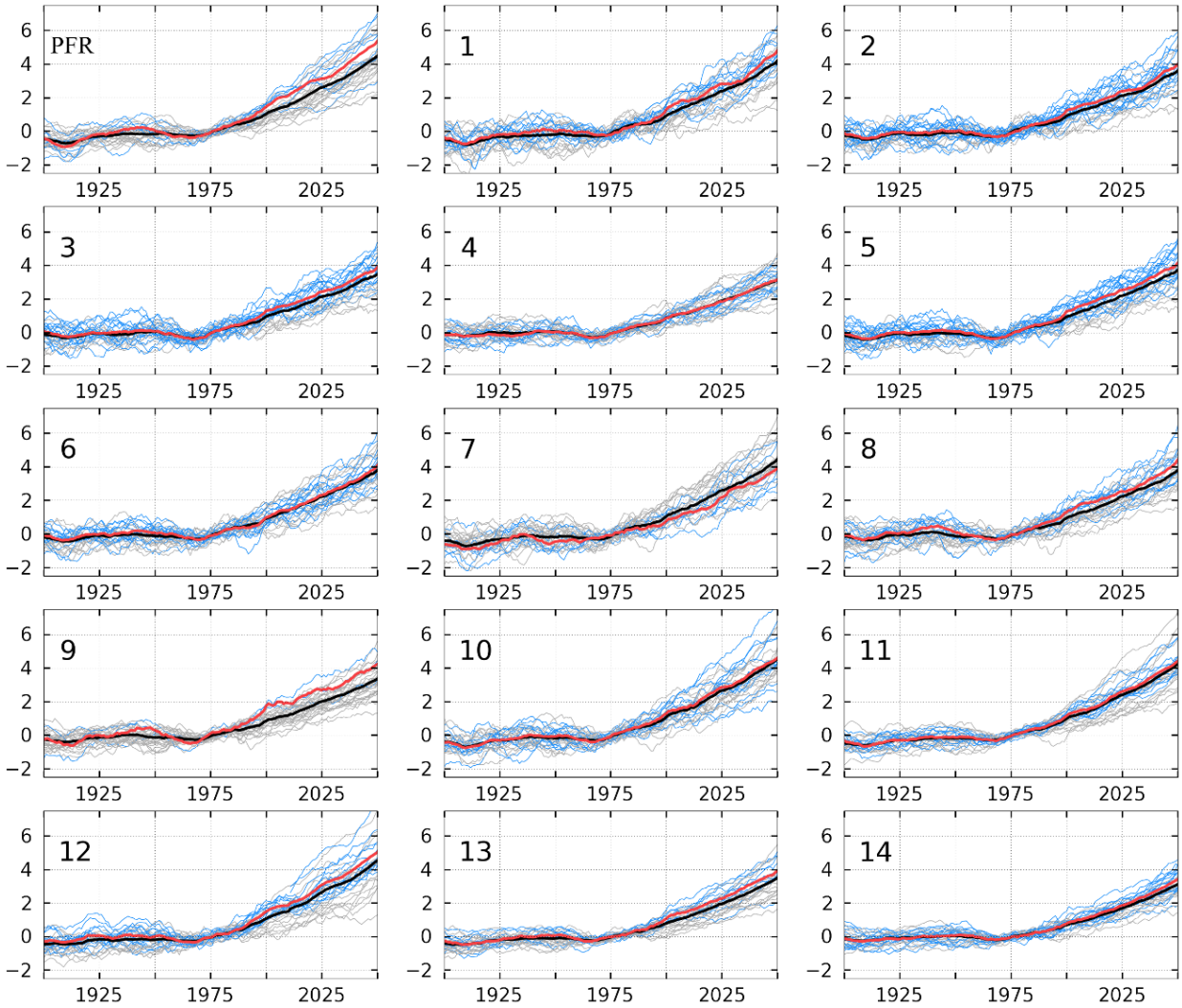

Fig. S3. Regional-mean MAAT projections from individual CMIP5 models (blue curves), ensemble of all 36 models (black curve), and optimal ensemble of models with the best regional skills (red curve).

Table S1 illustrates the disparity between the modeled MAAT trends and observations in the 1976-2005 period for selected regions in the Russian North and in the areas underlain by permafrost. Although not shown in the table, similar results were obtained for other climatic parameters and indexes. Models are classified by their relative errors, defined as the ratio of the difference between the calculated and observed trends of any given climatic parameter to their sum. The threshold for the relative error is set at 0.25 to distinguish between the highly accurate models and those that poorly represent observed regional trends. We eliminated outliers and combined the remaining twenty-nine “best” models into an “optimal ensemble.”

Some questions remain open, such as how to treat models that demonstrate a high accuracy with respect to certain climatic parameters in one region but perform poorly when other parameters in other regions are considered. These instances are displayed as grey cells in Table S2, which indicate that the relative model error is above the prescribed threshold for at least one of all tested parameters in the corresponding region.

Plots in Figure S3 show the variety of regional-mean MAAT projections from individual CMIP5 models (light blue curves), the ensemble of all 36 models (black curve), and the optimal ensemble of models with the best regional accuracy (red curve) for selected regions in the Russian North, including the areas underlain by permafrost. Hereafter, predictive CMIP5 model runs have been used for the 21st century under the high greenhouse gas emission scenarios likely to result from the developing world economy (RCP-8.5). Interestingly, except for Western Siberia (region 7), the optimal ensemble predicts higher rates of warming than the average over all models. Although the differences between the ensemble-means are small, the optimal ensemble has an added value in narrowing the range of uncertainty in climate projections by eliminating those based on ESMs with poor regional accuracy.

To further reduce the uncertainty, we eliminated the biases of individual models by combining their results with observations. We used each of the ESM results to calculate differences between the climatic indexes averaged over the 2036--2065 and 1961--1990 periods, and overlaid these differences with the baseline (1961--1990 mean) values calculated from the CRU TS3.10 gridded dataset.

Mathematical formalism of the SHI dynamical permafrost model

The dynamical permafrost model is based on the heat balance equation of the soil surface, heat transfer equation in snow and soil, and water balance equation:

$$c_e \frac{\partial T}{\partial t} = \frac{\partial}{\partial z}\left(\lambda \frac{\partial T}{\partial z} \right) + \rho_w L \frac{\partial W}{\partial t} \vartheta \qquad (1)$$

$$\frac{\partial W}{\partial t} = \frac{\partial}{\partial z}\left(K \frac{\partial \psi}{\partial z} - K \right) \qquad (2)$$

where $$c_e = \rho_w c_w + \rho_i c_i + \rho_s c_s (1 - P) + \rho_w L \frac{\partial W_l(T)}{\partial T} \vartheta ; \qquad (3)$$

$$\vartheta = \begin{cases} 0; \ if \ \ T \geq 0 \\ 0; \ if \ \ T < 0 \ \ and \ \ W \leq W_l(T) \\ 1; \ if \ \ T < 0 \ \ and \ \ W > W_l(T) \end{cases}$$

The following designations are used in (1) – (3): L – latent heat (j g^{-1}); T - soil temperature (°C); W,P – volumetric soil moisture and soil porosity (%); $W_l(T)$– unfrozen soil water content (g m^{-3}); ψ - soil moisture potential (m); K, λ– soil water conductivity (m s^{-1}) and thermal conductivity (w m^{-1} °C^{-1}) почвы; c_e – effective heat capacity of soil (j g^{-1} °C^{-1}); c_w,c_i, c_s and ρ_w, ρ_i, ρ_s, – heat capacity (j g^{-1} °C^{-1}) and density (g m^{-3}) of water, ice, and dry soil; ϑ - binary coefficient; t, z – time (s) and depth (m).

The heat transfer equation (1) accounts for the unfrozen water in soil pore space.

References

Anisimov, O. and V. A. Kokorev. 2017. Cities of the Russian North in the Context of Climate Change. Pages 141-174 *in* R. Orttung, editor. Sustaining Russia's Arctic Cities: Resource Politics, Migration, and Climate Change. Berghahn Books, New York.

Flato, G., J. Marotzke, B. Abiodun, P. Braconnot, S. C. Chou, W. Collins, P. Cox, F. Driouech, et al. 2013. Evaluation of Climate Models. Pages 741–866 *in* T. F. Stocker, D. Qin, G.-K. Plattner, M. Tignor, S. K. Allen, J. Boschung, A. Nauels, Y. Xia, et al., editors. Climate Change 2013: The Physical Science Basis. Contribution of Working Group I to the Fifth Assessment Report of the Intergovernmental Panel on Climate Change. Cambridge University Press, Cambridge, United Kingdom and New York, NY, USA.

Raisanen, J. and J. S. Ylhaisi. 2011. How Much Should Climate Model Output Be Smoothed in Space? Journal of Climate **24**:867-880.

Taylor, K. E., R. J. Stouffer, and G. A. Meehl. 2011. An Overview of CMIP5 and the Experiment Design. Bulletin of the American Meteorological Society. **93**:485-498.